Macromolecules
ARTICLE

*Macromolecules* **2010**, *43*, 2371–2376 **2371**
DOI: 10.1021/ma9025338

# Syndiotactic Polystyrene Nanofibers Obtained from High-Temperature Solution Electrospinning Process

**Yong-Wen Cheng,[†] Hsin-An Lu,[†] Yin-Chi Wang,[†] Annette Thierry,[‡] Bernard Lotz,[‡] and Chi Wang*,[†]**

[†]*Department of Chemical Engineering, National Cheng Kung University, Tainan 701, Taiwan, and* [‡]*Institut Charles Sadron (CNRS and ULP), Campus CNRS, 23, Rue du Loess, BP84047, 67034 Strasbourg, France*

*Received November 17, 2009; Revised Manuscript Received January 6, 2010*

ABSTRACT: Electrospun syndiotactic polystyrene (sPS) fibers with a diameter of 150−400 nm were successfully prepared via high-temperature electrospinning of solutions with different concentrations in an *o*-dichlorobenzene solvent. From the polarized FTIR spectra, the sPS chains in the as-spun fibers were amorphous and exhibited a preferential chain orientation along the fiber axis. Upon thermal annealing at a temperature lower than 270 °C, sPS crystals with the α-form modification were developed, as revealed by the electron diffraction patterns of the individual fiber segments. The orientation factor of the (002) plane was determined to be 0.94−0.97, relatively independent of the annealing temperature. Solvent-induced crystallization readily took place in these submicrometer-sized fibers, giving rise to the δ-form sPS crystals, as revealed by the FTIR spectra and WAXD patterns. The absorbed solvents could subsequently be expelled by boiling in ethanol, leaving the cavities available for the next solvent treatment. In contrast with the bulk films, sPS fiber mats exhibit a promising application in chemical separation and water purification due to their large surface area as well as high solvent permeation resulting from its small-fiber diameter character.

## 1. Introduction

Driven by the widespread interest in nanofiber application, solution electrospinning has become a fascinating technique to prepare polymeric fibers. By carefully controlling the solution properties (viscosity, conductivity, and surface tension), the processing variables (applied voltage, flow rate, and tip-to-collector distance), and the spinning environments (humidity and temperature), electrospun fibers with desirable diameters ranging from 50 to 1000 nm can be readily obtained. Many related articles and review monographs have already discussed the processing details and the microstructure of electrospun fibers.[1−8] However, the development of high-temperature electrospinning solutions is still slow. There have only been a few articles that report solution temperature effects on electrospinnability.[9−11] Not only can solution electrospinning at elevated temperatures further reduce the fiber diameter, because of the low solution viscosity for processing, it is also a "must" for most of the semicrystalline polyolefins which cannot be dissolved at ambient temperature. By means of a heating jacket to control the solution temperature,[12] we succeeded in performing solution electrospinning at temperatures of up to 90 °C. In this study, we further extended this design by coupling electrospinning with an IR emitter in an attempt to control the electrospinning environmental temperature. The success of electrospinning in syndiotactic polystyrene (sPS) solutions, and the microstructure of the electrospun fibers, as well as the potential application of these sPS fiber mats, will be presented and discussed.

In contrast with atactic PS, sPS is a semicrystalline counterpart with a high melting temperature (∼270 °C). Because of its polymorphic nature, sPS exhibits several different crystal modifications, depending upon the crystallization conditions.[13,14] Among them, the clathrate (δ) form induced from the solution state by solvent inclusion in the crystal modification has received much attention due to its potential application in chemical separation and water purification.[15−17] The incorporated solvent molecules are located in the interstitial cavities of the sPS crystals and can be extracted by suitable solvent treatments without significantly changing the cavity dimensions. This gives rise to the $\delta_e$ form of the crystals. The $\delta_e$-form crystals can be used to reabsorb desirable solvents, provided that the solvent size is smaller than the cavity dimensions.[15] By means of repetitive absorption and desorption, sPS samples with the clathrate structure provide a feasible route for chemical separation. Most of the previous studies used dense sPS thin films to fulfill this application. It has been noted that the solvent molecules have to diffuse from the film surface into the "guest site" located in the host sPS crystallites. In general, a thicker film is desirable since more $\delta_e$-form crystals are provided to include more solvents, but the solvent diffusion may become a time-consuming process if the film thickness is too large. To increase the effectiveness of solvent absorption/desperation, the use of mats made of sPS nanofibers are appropriate due to their porous structure as well as large surface area. Our electrospun sPS fiber mats fulfilled the application requirements of high flux rate and large surface area.

## 2. Experimental Section

**Electrospinning of sPS Solution.** The sPS pellets were supplied by The Dow Chemical Company. The weight-average molecular weight ($M_w$) and the polydispersity were 225 800 g/mol and 2.11, determined by a high-temperature gel permeation chromatograph (GPC) (Waters Alliance, GPVC2000) at 140 °C using 1,2,4-trichlorobenzene as the mobile fluid. The apparent glass transition and melting temperatures were 95 and 269 °C, respectively, using differential scanning calorimeter (Perkin-Elmer, DSC7) on the melt-quenched sample at a heating rate of 10 °C/min. Atactic PS pellets with an $M_w$ of 300 000 g/mol

*Corresponding author: Tel +886-6-2757575 ext 62645; Fax +886-6-2344496; e-mail chiwang@mail.ncku.edu.tw.



Published on Web 02/04/2010

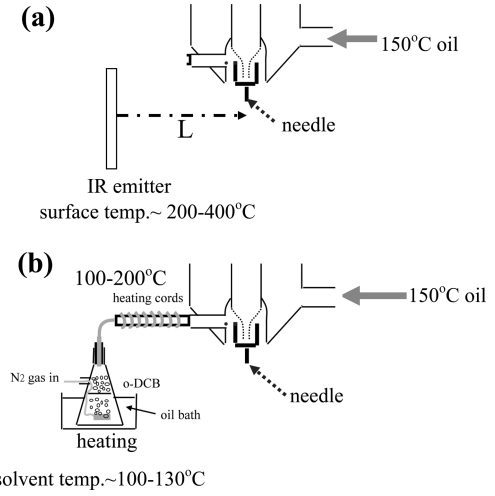


**Figure 1.** Schematic diagrams for controlling the temperature of needle end during the high-temperature electrospinning process: (a) an IR emitter with a desired distance of $L$ to provide radiation energy for maintaining needle-end temperature above $T_{gel}$; (b) superheated *o*-DCB vapors introduced by $N_2$ carrier gas to encapsulate the needle end for preventing the temperature drop lower than $T_{gel}$ as well as severe solvent evaporation.

were provided by Chi-Mei Corp. (Taiwan). *o*-Dichlorobenzene (*o*-DCB) was used to prepare the homogeneous solutions for electrospinning. Because of the low conductivity of sPS/*o*-DCB solutions, electrospun products in the absence of fiber features were obtained despite the presence of chain entanglements in the solution state. To enhance the conductivity of solution, tetra-*n*-butylammonium perchlorate was added, and electrospun fibers could be readily seen afterward. In some occasions, more conductive dimethylformamide (DMF) solvent was mixed with *o*-DCB to prepare the sPS solution; however, this cosolvent system was not effective due to the limited solubility of sPS in DMF, leading to the phase separation of the prepared solutions.

To prepare solutions with different wt % concentrations, weighted amounts of sPS and *o*-DCB were mixed at 140 °C for 2 h until homogeneous solutions were obtained. Similarly, sPS/aPS blend solutions with different weight ratios under a given polymer concentration of 14 wt % were also prepared for the composite fibers. For the neat and blend solutions, the concentration of 0.5 wt % of added salt was relative to the mass of the solvent used. Figure 1 shows the schematic diagram of the high-temperature electrospinning system. A homemade jacket-type heat exchanger was used to maintain the polymer solution at a desirable electrospinning temperature. This was fulfilled via the circulation of heated silicone oil by a pumping system connected to an oil bath where temperature could be adjusted up to 150 °C. Because of its "one-dimensional fin" geometry, a significant temperature gradient was found along the needle, giving rise to an apparent temperature difference for solutions within the jacket tube and at the needle end. This temperature drop eventually led to gel formation at the surface of the Taylor cone adjacent to the needle end. A needle with a thin wall was found to be able to better prevent the stagnant flow in the Taylor cone beneath the needle base, where gel initiation took place. Once the initially small amount of gel was adhered to at the needle base, it gradually grew and finally blocked the main stream flow in the Taylor cone, leading to the cone distortion and an uncontrolled electrospinning process. To prevent and resolve the gel formation problem, either an IR emitter (Figure 1a)[9] or an "*o*-DCB vapor generator" (Figure 1b)[12] was used to maintain the solution at a sufficiently high temperature. By adjusting the power of the IR emitter and its distance from the needle, the solution temperature at the needle end was varied. Similarly, *o*-DCB vapor with a predetermined temperature was delivered

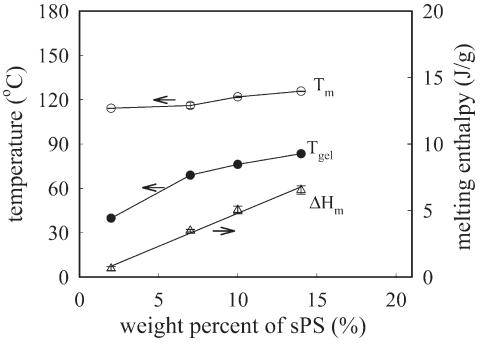


**Figure 2.** sPS concentration dependence of gel formation temperature, $T_{gel}$, gel melting temperature, $T_m$, and the gel melting enthalpy, $\Delta H_m$.

using a controlled flow rate of $N_2$ carrier gas to blanket the Taylor cone without interrupting the bending instability (Figure 1b). It should be noted that solvent evaporation might be significantly enhanced when the solution temperature approaches the boiling temperature of the solvent used (180.5 °C for *o*-DCB), resulting in a gradual cone shrinkage and leading to an unstable electrospinning. For our designed apparatus, a cone-jet electrospinning mode could be smoothly performed on the sPS solutions at temperatures of up to 110 °C. By measuring the temperature of the pendant drop at the needle end using a thermocouple, the solution working temperature for electrospinning was determined. When the system reached thermal equilibrium, the homogeneous polymer solution was electrospun into the fiber forms according to the procedure previously reported.[12]

**Characterization of Solution and Fibers.** Gel formation at the needle base will alter the streamline in the Taylor cone and eventually clog the solution flow, resulting in process interruption. It is important to determine the temperature range of processing prior to electrospinning to eliminate gel formation. Calorimetric measurements were carried out using a Perkin-Elmer DSC7 at scanning rates of 2, 5, and 10 °C/min to cool the homogeneous sPS solutions to room temperature. The gel formation temperature ($T_{gel}$) was determined by temperature extrapolation of the exothermic peak to a rate of 0 °C/min. The melting temperature of gel ($T_m$) was determined from the endothermic peak using a heating rate of 10 °C/min, and the corresponding melting enthalpy ($\Delta H_m$) represented the gel content.

The nanofibers were shadowed with Pt/C to coat a carbon layer, backed with a poly(acrylic acid), floated on water, mounted on a copper grid, and then examined via a Philips CM12 electron microscope operating at 120 kV. The morphology and diameter of the electrospun fibers were also observed using a scanning electron microscope (SEM, Hitachi S4100). Annealing of sPS fibers was performed in a Mettler FP900 hot stage. Infrared spectra were obtained by a Perkin-Elmer Spectrum 100 spectrometer at 128 scans with a resolution of 2 $cm^{-1}$. To investigate the influence of solvent vapor, a homemade chamber similar to that used by Tashiro et al.[18] was constructed to obtain the *in situ* FTIR spectra of as-spun fibers exposed to the given solvent vapor. Wide-angle X-ray diffraction (WAXD) patterns were obtained in transmission mode with graphite-monochromatized Cu Kα radiation using a Bruker diffractometer (NanoSTAR Universal System).

## 3. Results and Discussion

sPS solutions have the tendency to form gels.[14] Understanding the gel formation temperature, gel content, and its melting temperature is a critical step in controlling the electrospinning process. As can be seen from Figure 2, $T_{gel}$ and $T_m$ increase along with increasing sPS concentration. In addition, gel content also increases linearly with the sPS concentration. The FTIR results

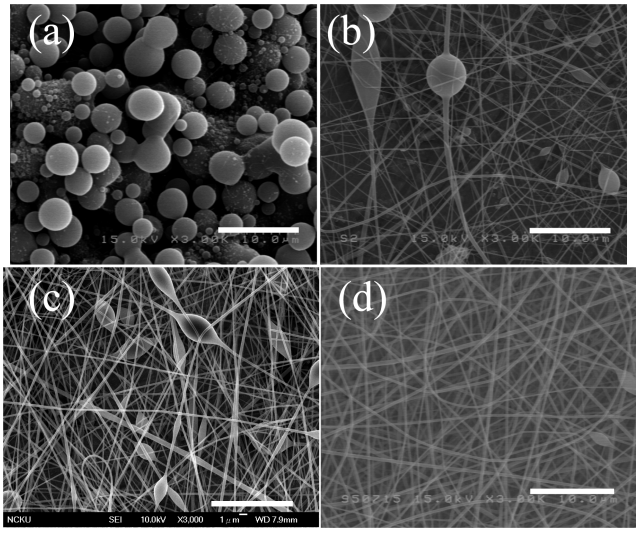


**Figure 3.** Morphologies of sPS fibers electrospun from solutions of (a) 7, (b) 12, (c) 14, and (d) 14 wt %: (a−c) obtained by IR heating and (d) by superheated *o*-DCB vapor to control the needle-end temperature. The scale bar is 10 $\mu$m.

showed that these sPS gels possessed the $\delta$-form crystals with TTGG conformation together with an excess amount of *o*-DCB solvent. In addition, the sPS gel became more rigid when sPS content in the solution was higher. Based on this phase diagram, the temperature of the electrospinning solution should be maintained at a temperature higher than $T_{gel}$ in order to perform a smooth process.

It has been shown that solutions with a sufficient entanglement density are required to prepare uniform electrospun fibers.[19,20] For a given MW of polymers, the entanglement concentration ($c_e$) could be estimated by the equation $c_e = M_c/M_w \sim 2M_e/M_w$, where $M_c$ and $M_e$ are the critical molecular weight and entanglement molecular weight of polymer, respectively, in the melt state. Although Fetter et al.[21] recently pointed out the incorrectness of the perceived kinship of $M_c \sim 2M_e$, this simple equation provides a rule of thumb when sufficient data are not available. It should be noted that $M_e$ depends on the polymer type and is relatively independent of the solution temperature. Since no $M_e$ has yet been reported for sPS in the available literature, we tentatively used that of aPS ($M_c$ = 31 200, $M_e$ = 18 100 g/mol)[21] for the present estimation. The calculated value of $c_e$ is 13.9 vol % (~11.6 wt %). Previous studies have shown that $c_e$ represents the minimum concentration for electrospun products exhibiting fiberlike structures. Depending upon the entanglement strength in the solution state, solutions with a concentration ca. 1.5−2.0$c_e$ are generally required for producing uniform polymer fibers.[19,20] On the other hand, solutions with a concentration lower than $c_e$ will only yield polymer particulates.

Figure 3 shows the electrospun products obtained from solutions with different sPS concentrations; our findings are consistent with the theoretical consideration; that is, only sPS beads with a diameter of 1.6−5.0 $\mu$m are obtained for the 7 wt % solutions (Figure 3a). However, sPS fibers with several beads-on-a-string structure were seen when the sPS concentration is larger than $c_e$ (Figure 3b,c). In addition, it is evident that more uniform sPS fibers are obtained by introducing a "solvent vapor" instead of using an IR emitter (Figure 3c,d). In other words, the former is more effective because of the "localized heating" and encapsulation of the cone surface, which prevents significant solvent evaporation at elevated temperatures. On the other hand, the latter increases not only the temperature of the Taylor cone but also the electrospinning environment, which profoundly enhances solvent evaporation during jet whipping. Thus, the

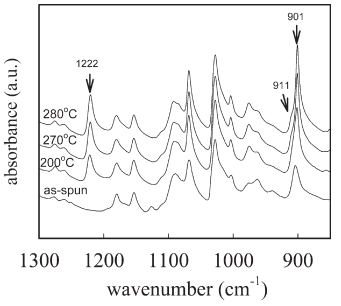


**Figure 4.** FTIR spectra of the as-spun sPS fiber and that annealed at different temperatures. The band at 1222 cm$^{-1}$ is associated with the TTTT chain conformation in the crystals, whereas 901 and 911 cm$^{-1}$ are associated with the α-form and $\beta$-form crystals, respectively.

morphology of collected fibers, depending upon the "localized jet stretching" and "solvent evaporation history", varies significantly from one to the other. We concluded that the setup using the superheated *o*-DCB vapors (Figure 1b) to keep the needle temperature sufficiently high to eliminate the gel formation is the preferred design. When the 14 wt % solution was electrospun, the fiber diameters ranged from 100 to 400 nm, and the average fiber diameter was 178 ± 59 nm. The average fiber diameter was found to increase with increasing sPS concentration; for example, electrospinning a 25 wt % solution yielded sPS fibers with a diameter of ~1190 ± 340 nm.

sPS is a polymorphic material possessing various crystal modifications, typically the α-form with hexagonal, the $\beta$-form with orthorhombic, and both $\gamma$- and $\delta$-forms with monoclinic lattices.[13,14,22−24] Both α- and $\beta$-forms are mainly derived from melt crystallization, whereas the $\gamma$- and $\delta$-forms are obtained from solvent-induced crystallization. It has been demonstrated that the absorbance peak at 1222 cm$^{-1}$ is associated with the crystalline phase, with TTTT chain conformation existing in the α- and $\beta$-form sPS. On the other hand, both $\gamma$- and $\delta$-forms give rise to the characteristic band of TTGG chain conformation at 572 cm$^{-1}$. In the absence of these characteristic bands (Figure 4), the as-spun sPS fibers were found to be amorphous due to the rapid solvent evaporation resulting from the high-temperature electrospinning process. Thermal treatments on the as-spun amorphous fibers were performed at various $T_c$, and the corresponding FTIR spectra are also displayed in Figure 4 to detect the variation of fiber microstructures. Three absorbance peaks are seen in the 870−920 cm$^{-1}$ range, and the corresponding peaks at 901, 911, and 906 cm$^{-1}$ are attributed to the α-form, the $\beta$-form, and the amorphous phase, respectively. After being held at 200 °C for 2 h, the as-spun sPS fibers undergo cold crystallization and give rise to the α-form crystals, evidenced by the appearance of 901 and 1222 cm$^{-1}$ bands. When the as-spun fibers are rapidly raised to 270 °C, followed by a cooling rate of 10 °C/min to room temperature, some trace of $\beta$-form crystals is identified from the presence of absorbance shoulder at 911 cm$^{-1}$. More $\beta$-form crystals are developed when the fibers are shortly annealed at temperatures of up to 280 °C. The crystal transformation in the sPS fibers, from the amorphous phase to the α form at low annealing temperatures and to the α/$\beta$-mixed form at high annealing temperatures (> 270 °C), has also been confirmed by the electron diffraction technique conducted on the single fiber. Under EM observations, sPS fibers that experienced 280 °C annealing showed a partial melting of the skin layer, whereas those annealed below 270 °C kept their round shape.

Aligned sPS fiber bundles were collected using two parallel electrodes, which introduced an interacting electric field to force the charged fibers to lie across them. The gap between electrodes was 10 mm. In addition, bundles with relatively well-aligned fibers were also obtained by electrospinning the fibers into a

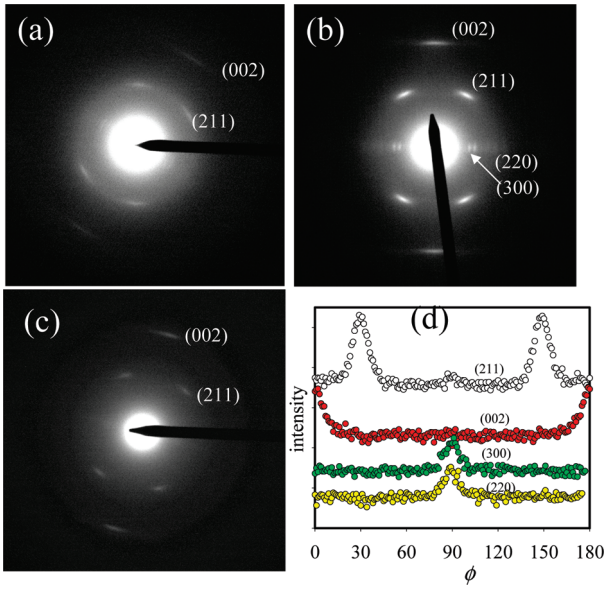


**Figure 5.** ED patterns of annealed sPS fibers thermally treated (a) at 240 °C for 6 h by heating the as-spun fibers at a rate of 2 °C/min, (b) at 260 °C for 2 h by heating the as-spun fibers at a rate of 100 °C/min to 270 °C and rapidly cooling down to 260 °C, (c) sPS/aPS 1/1 composite fibers at 260 °C for 2 h using the same treatment for the neat sPS fiber, and (d) azimuthal angle dependence of intensity profiles of image b. The calculated values of $f_{c,Z}$ values by the (002) plane are 0.98, 0.98, and 0.94 for the images of (a), (b), and (c), respectively.

nonsolvent (e.g., water) bath and being rapidly picked and aired by a collecting device through the help of capillary force.[25] These aligned fibers were shed by the polarized IR light with the electric vector parallel and perpendicular to the fiber axis to determine the respective absorbances (i.e., $A_{\parallel}$ and $A_{\perp}$). The determined dichroic ratio ($A_{\parallel}/A_{\perp}$) of the 906 $cm^{-1}$ band (benzene stretching) was 1.21, suggesting that a chain orientation has been preferentially developed in the amorphous fibers. It should be noted, however, that the fiber alignment in the bundle was not perfect, and the derived dichroic ratio represents only the global orientation of the fibers and chain orientation in the fibers. With the help of a small beam size, ED was applied to investigate the chain orientation in the *individual* nanofibers. Being consistent with FTIR results (Figure 4), our as-spun nanofibers exhibited a featureless ED pattern, suggesting that crystallization was completely inhibited during the electrospinning, which is also in agreement with the WAXD results (Figure 7). The as-spun fiber presents a good model fiber to understand the crystallization behavior of sPS chains induced from the amorphous and orientated states. In the following section, thermal treatments on as-spun sPS fibers are performed, and the modification and orientation of the induced crystals in each *individual* fiber are investigated by the ED technique.

Figure 5 shows the typical ED patterns of the as-spun fibers annealed at different temperatures and given sufficient time to complete crystallization. When fibers were directly heated to $T_c$ for cold crystallization, most ED patterns showed the absence of equatorial intensity profiles, whereas diffraction distances of 0.435 and 0.252 nm were clearly observed in the first and second layers, respectively (Figure 5a). The former was relevant with the (211) plane, and the latter was attributed to the (002) plane of the α-form. The ED intensity profiles further suggest that mesomorphic sPS forms (imperfect α crystals)[26] were developed within the annealed fibers. However, when the as-spun fibers were rapidly heated to 270 °C and quickly cooled down to $T_c$, the ED patterns became more intense (Figure 5b), in which the equatorial profiles show the diffraction distances of 0.657 and 0.758 nm, corresponding to the (220) and (300) planes of the α crystals, respectively.

The sPS/aPS composite nanofibers were also electrospun from the high-temperature solution process using sPS/aPS/*o*-DCB solutions with various sPS/aPS weight ratios. The as-spun composite fibers were also amorphous. For the sPS/aPS 9/1 composite fibers, similar ED patterns, as those shown in Figure 5b, were seen. For the sPS/aPS 1/1 fibers (Figure 5c), characteristic diffractions of the (211) and (002) planes were still seen, but the equatorial intensity profiles were absent due to the low crystallinity developed within the composite fibers. We concluded that α-form crystals were preferentially developed after annealing the as-spun amorphous sPS (or sPS/aPS) nanofibers at temperatures lower than 270 °C. The orientation factor of the induced crystals was determined using the Herman orientation function:[27]

$$f = (3\langle\cos^2\phi_{hkl,Z}\rangle - 1)/2 \quad (1)$$

where $\langle\cos^2\phi_{hkl,Z}\rangle$ is the squared average of cosine value of the angle, $\phi_{hkl,Z}$, between the normal of (*hkl*) plane with the fiber axis (*Z*-axis). The quantity can be experimentally derived by the equation

$$\langle\cos^2\phi_{hkl,Z}\rangle = \int_0^{\pi/2} I_{hkl}(\phi)\cos^2\phi\sin\phi\,d\phi \Big/ \int_0^{\pi/2} I_{hkl}(\phi)\sin\phi\,d\phi \quad (2)$$

where $I_{hkl}(\phi)$ is the intensity distribution of (*hkl*) plane on the Debye ring and $\phi$ is the azimuthal angle measured from the meridian (fiber axis direction). Perfect crystal orientation leads to the $f_{c,Z}$ value of 1.0, whereas perpendicular crystal orientation gives rise to a value of −0.5. Figure 5d shows the intensity profiles of different planes along the azimuthal direction of the Figure 5b image. Using the (002) intensity profile, the crystal *c*-axis orientation, $f_{c,Z}$, could be directly determined. In addition, the following equation may be applied from the (*hk*0) intensity profile to verify the derived one by the (002) plane

$$\langle\cos^2\phi_{c,Z}\rangle = 1 - 2\langle\cos^2\phi_{hk0,Z}\rangle \quad (3)$$

Similar values of $f_{c,Z}$ were obtained irrespective of the diffraction planes applied. For a given annealed sample, however, the determined $f_{c,Z}$ is sometimes different from one fiber segment to another selected for ED analysis. This is attributed to the intrinsic difference in the chain alignment developed in the as-spun amorphous fiber because the electrospinning jets experience different levels of electric stretching during the whipping process. Regardless of the annealing temperatures, however, the highest value of $f_{c,Z}$ determined from several selected single fibers was mainly in the range of 0.97−0.98, suggesting the development of highly oriented α-form crystals in the nanofibers after thermal annealing. In other words, the prealigned amorphous chains in the as-spun nanofibers rapidly undergo crystallization prior to the chain relaxation when the annealing temperature is lower than 270 °C. For the annealed composite fibers, the presence of an aPS component with a content up to 50 wt % leads to a slight reduction of crystal orientation to a $f_{c,Z}$ value of 0.94 (Figure 5c).

Amorphous sPS thin films will absorb suitable solvents to form clathrates possessing the δ-form crystals with the solvent included in the crystals.[14] Similar absorption behavior was observed in our electrospun sPS fiber mats when immersed in the solvent liquids. Figure 6a shows the typical FTIR spectra of the as-spun sPS fibers before and after immersing in toluene liquid for 30 s, followed by pumping under vacuum at room temperature to remove the toluene in the amorphous region. The appearance of

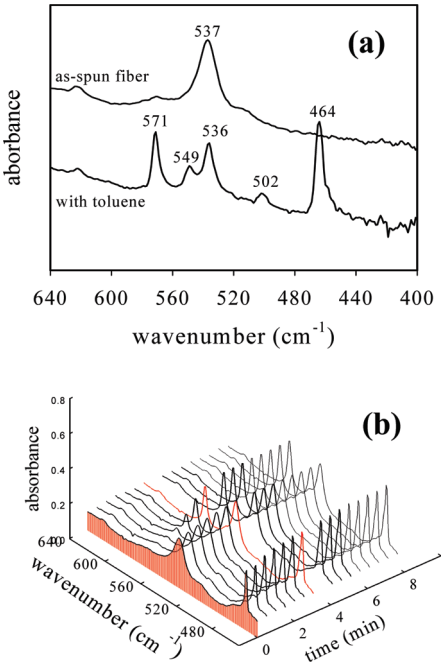


**Figure 6.** (a) FTIR spectra of sPS fibers before and after the treatment of toluene liquid. (b) In-situ FTIR spectra of as-spun sPS fibers exposing to the toluene vapor. The band at 571, 549, and 502 $cm^{-1}$ are associated with the TTGG chain conformation in the $\delta$-form crystal.

typical bands at 571, 549, and 502 $cm^{-1}$ indicates the formation of TTGG chain conformation in the developed crystals. Together with the presence of a toluene band at 464 $cm^{-1}$, the induced crystals are verified to be in the $\delta$-form. Because of its small diameter and porous structure, our as-spun sPS fibers are able to rapidly absorb many other solvent liquids, such as chloroform, cyclohexane, ethyl acetate, and DMF, provided that the size of the solvent molecule is smaller than the dimensions of the interstitial cavities of the crystals.[15] These absorbed molecules act as plasticizers to reduce $T_g$ and transform the amorphous sPS chains into the helical ordered structure, leading to the formation of clathrate ($\delta$-form). To trace the microstructure transformation by the vapor, instead of liquid, *in situ* FTIR measurements were performed by exposing the as-spun fiber mats to a saturated vapor of different solvents at room temperature. sPS clathrates with different solvents included in the crystals were also obtained, but a longer time was required for the crystal transformation, compared to the application of liquid. Figure 6b shows the time dependence of IR spectra of sPS fibers exposed to toluene vapor at room temperature. After a very short induction time, transformation from the amorphous to clathrate rapidly takes place to reach saturation. Our present study on the electrospun sPS indicates that the time required for the solvent-induced crystallization is significantly reduced when compared to that for the condensed sPS thin film.[18] Figure 7 exhibits the WAXD intensity profiles of different sPS clathrates after the treatment of different vapors. Also included is the WAXD pattern of the as-spun fiber mats, which merely shows the amorphous halo. After vapor treatment, the diffraction peaks at $2\theta = 8.4°$ and $2\theta = 10.0°$ are the fingerprints of the $\delta$-form sPS,[14,23,24] which correspond to the (010) and ($\bar{2}$10) reflections, respectively. Additional broad diffraction peaks at $2\theta = 15.8°$, 19.5°, and 23.5° are also discernible. These WAXD patterns are rather similar since these clathrates all possess a similar unit cell.[17,28] On the basis of the FTIR and WAXD results, we concluded that the oriented amorphous chains in the as-spun sPS fibers with a diameter of 200−800 nm are able to crystallize into the $\delta$-form crystals under the influence of a solvent liquid (or vapor). When these $\delta$-form sPS fibers are

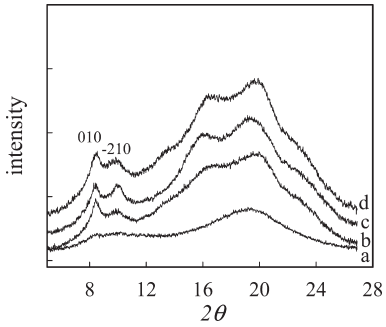


**Figure 7.** WAXD intensity profiles of the as-spun sPS fibers (curve a). sPS fibers exposed to different solvent vapors: toluene (curve b), *o*-DCB vapor (curve c), and *p*-xylene (curve d).

treated using boiling ethanol, the entrapped solvent molecules in the crystalline region are successfully removed from the cavities. With the advantage of a larger surface area and porous interior, the electrospun sPS fiber mat is a potentially more efficient media than condensed sPS thin films for application in chemical separation and water treatment.

## 4. Conclusions

High-temperature electrospinning of sPS solutions became feasible by using a jacket-type heat exchanger to control the solution temperature. To prevent gel formation, which clogs the Taylor cone, the solution temperature was kept above the gel formation temperature but below the temperature at which significant solvent evaporation takes place. Two heating approaches, specifically IR emitter and superheated *o*-DCB vapor, were designed for maintaining the spinneret temperature to prevent gel formation at the Taylor cone. It was found that introduction of a saturated *o*-DCB vapor is more effective than using an IR emitter for reducing the level of solvent evaporation. The as-spun sPS fibers were amorphous. After annealing at temperatures below 270 °C, highly oriented crystals with the α-form modification were developed. In addition, under suitable solvent treatment at room temperature, the amorphous sPS chains rapidly crystallized to form the sPS clathrate. The included solvents could be removed by boiling ethanol. By repetitive absorption and desorption of the desired solvent liquids (or vapors), these sPS fiber mats with clathrate structure are promising in the application of chemical separation.

**Acknowledgment.** This work was supported by the National Science Council of Taiwan (NSC94-2216-E-006-004, NSC96-2918-I-006-011) and the Landmark Project of National Cheng Kung University (B0147). C.W. thanks Drs. Lotz and Thierry for their hospitality during his stay in Strasbourg.

**Supporting Information Available:** SEM and polarized IR data of the as-spun fibers collected from the water bath; FTIR spectra of the sPS/*o*-DCB gels; crystal orientation factors of electrospun fibers annealed at different temperatures. This material is available free of charge via the Internet at http://pubs.acs.org.

## References and Notes

(1) Reneker, D. H.; Chun, I. *Nanotechnology* **1996**, *7*, 216.
(2) Huang, Z. M.; Zhang, Y. Z.; Kotaki, M.; Ramakrishna, S. *Compos. Sci. Technol.* **2003**, *63*, 2223.
(3) Li, D.; Xia, Y. *Adv. Mater.* **2004**, *16*, 1151.
(4) Ramakrishna, S.; Kazutoshi, F.; Teo, W. E.; Lim, T. C.; Ma, Z. In *An Introduction to Nanofibers*; World Scientific Co. Pte. Ltd.: Singapore, 2005.

(5) Reneker, D. H.; Fong, H. *Polymeric Nanofibers*; ACS Symposium Series 918; American Chemical Society: Washington, DC, 2006.
(6) Reneker, D. H.; Yarin, A. L.; Zussman, E.; Xu, H. In Aref, H., Van Der Giessen, E., Eds.; *Advances in Applied Mechanics*; Elsevier/Academic Press: London, 2007; Vol. *41*, pp 43−195.
(7) Greiner, A.; Wendorff, J. H. *Angew. Chem., Int. Ed.* **2007**, *46*, 5670.
(8) Reneker, D. H.; Yarin, A. L. *Polymer* **2008**, *49*, 2387.
(9) Givens, S. R.; Gardner, K. H.; Rabolt, J. F.; Chase, D. B. *Macromolecules* **2007**, *40*, 608–610.
(10) Rein, D. M.; Shavit-Hadar, L.; Khalfin, R L.; Cohen, Y.; Shuster, K.; Zussman, E. *J. Polym. Sci., Polym. Phys. Ed.* **2007**, *45*, 766–773.
(11) Desai, K.; Kit, K. *Polymer* **2008**, *49*, 4046–4050.
(12) Wang, C.; Chien, H. S.; Hsu, C. H.; Wang, Y. C.; Wang, C. T.; Lu, H. A. *Macromolecules* **2007**, *40*, 7973.
(13) Woo, E. M.; Sun, Y. S.; Yang, C. P. *Prog. Polym. Sci.* **2001**, *26*, 945–983.
(14) Gowd, E. B.; Tashiro, K.; Ramesh, C. *Prog. Polym. Sci.* **2009**, *34*, 280–315.
(15) Milano, G.; Venditto, V.; Guerra, G.; Cavallo, L.; Ciambelli, P.; Sannino, D. *Chem. Mater.* **2001**, *13*, 1506–1511.
(16) Gowd, E. B.; Shibayama, N.; Tashiro, K. *Macromolecules* **2006**, *39*, 8412–8418.
(17) Chatani, Y.; Shimane, Y.; Inagaki, T.; Ijitsu, T.; Yukinari, T.; Shikuma, H. *Polymer* **1993**, *34*, 1620–1624.
(18) Tashiro, K.; Ueno, Y.; Yoshioka, A.; Kobayashi, M. *Macromolecules* **2001**, *34*, 310–315.
(19) McKee, M. G.; Wilkes, G. L.; Colby, R. H.; Long, T. E. *Macromolecules* **2004**, *37*, 1760–1767.
(20) Shenoy, S. L.; Bates, W. D.; Frisch, H. L.; Wnek, G. E. *Polymer* **2005**, *46*, 3372.
(21) Fetters, L. J.; Lohse, D. J.; Milner, S. T.; Graessley, W. W. *Macromolecules* **1999**, *32*, 6847–6851.
(22) Guerra, G.; Vitagliano, V. M.; De Rosa, C.; Petraccone, V.; Corradina, P. *Macromolecules* **1990**, *23*, 1539.
(23) Manfredi, C.; De Rosa, C.; Guerra, G.; Rapacciuolo, M.; Auriemma, F.; Corradini, P. *Macromol. Chem. Phys.* **1995**, *196*, 2795–2808.
(24) Sun, Y. S.; Woo, E. M.; Wu, M. C. *Macromol. Chem. Phys.* **2003**, *204*, 1547–1556.
(25) Smit, E.; Buttner, U.; Sanderson, R. D. *Polymer* **2005**, *46*, 2419–2423.
(26) Auriemma, F.; Petraccone, V.; Dal Poggetto, F.; De Rosa, C.; Guerra, G.; Manfredi, C.; Corradini, P. *Macromolecules* **1993**, *26*, 3772–3777.
(27) Alexander, L. E. *X-ray Diffraction Methods in Polymer Science*; John Wiley & Sons: New York, 1969; p 241.
(28) Tarallo, O.; Petraccone, V. *Macromol. Chem. Phys.* **2005**, *206*, 672–679.